INTERACTION CURVES FOR CONCRETE-FILLED L-SHAPED MULTI-CELLED STEEL TUBE SECTIONS UNDER COMBINED BIAXIAL BENDING AND AXIAL FORCE

G.S. Tong* and X.G. Li

College of Civil Engineering and Architecture,
Zhejiang University, Hangzhou, Zhejiang Province, China
**(Corresponding author: E-mail: tonggs@zju.edu.cn)*

Received: 19 April 2018; Revised: 23 July 2018; Accepted: 25 July 2018

ABSTRACT: Ultimate yield surfaces of concrete-filled L-shaped multi-celled steel tube column (L-CFT) under biaxial bending and axial force are studied in this paper. The characteristics of the axial force-bending moment interaction curves under uniaxial bending is first revealed, while the rotational symmetry of the overall interaction curve is verified mathematically. Based on the relative positions of the elastic centroid axis and the plastic neutral axis under pure bending, six cases are identified whose interaction curves show slightly different features. The interaction curves between axial force and bending moments are grouped into two categories. Finally, the interaction surfaces of L-CFT under biaxial bending and axial force are analyzed. The characteristics of these curves are discussed and verified mathematically, and further the approximate formulas for design purpose are provided. Based on the comparative study of a large number of examples, the proposed formulas show good accuracy and are on the conservative side.

Keywords: Concrete-filled steel tube, multi-celled, strength, biaxial bending, interactive relation

DOI: 10.18057/IJASC.2018.14.11

1 INTRODUCTION

L-shaped, T-shaped and cruciform columns can be designed to be invisible at four corners of a room, making better use of living space, and therefore are welcomed by architects who need to meet the captious requirement of apartment buyers in their design work. In the case of reinforced concrete frames, the Ministry of Housing and Urban-Rural Development of China issued a technical specification (JGJ149-2006 [1]) to codify the application of such members and this specification was renewed in 2017. Such types of columns in reinforced concrete under biaxial bending had been experimentally and numerically investigated (Hsu [2-3]). The Structural analysis of frames built of such columns requires a slightly modified stiffness matrix where the product of inertia of the column cross section must be included (Sun [4]). Steel-reinforced concrete (SRC) columns of such special types have also been studied (Zhao [5]). Concrete-filled steel tube columns (CFT) are now the most frequently used members in high-rise buildings. It has high bearing capacity, excellent seismic and good fire-resistant behavior, is easy to construct and therefore relatively cost-effective. In the case of residential buildings, concrete-filled multi-celled L-shaped and T-shaped steel tube columns have been attracting the attention of structural engineers and researchers due to the same demand on living spaces.

As regards to the 3D ($P-M_{\mathrm{x}}-M_{\mathrm{y}}$) cross section strength, Chen and Atsuta [6] developed systematic approaches to find the section strength of steel under axial force and biaxial bending. For CFT members, Hajjar and Gourley [7] provided a perfect description on modeling of stress-strain relations of both steel and concrete and developed polynomial expressions to represent the three-dimensional surface for the section strength of rectangular CFTs, the proposed equations

may be applied in the pushover analysis. The China Association for Engineering Construction Standardization issued in 2004 a specification (CECS159-2004 [8]) on the design of CFT members, in deriving the design equations, the stress distribution in steel and concrete is based on full plasticity assumption. The effect of confinement of steel tube to concrete is assumed to produce only an increase in ductility of the concrete and no increase in strength. The stress in concrete is shown in Figure 1a, the interaction curves are shown in Figure 1b, and can be expressed by

$$\frac{P}{P_{\mathrm{P}}} \le \alpha_{\mathrm{c}} : \frac{M_{\mathrm{x}}}{M_{\mathrm{Px0}}} = 1 \tag{1a}$$

$$\frac{P}{P_{\mathrm{P}}} \ge \alpha_{\mathrm{c}} : \frac{P}{P_{\mathrm{P}}} + (1-\alpha_{\mathrm{c}})\frac{M_{\mathrm{x}}}{M_{\mathrm{Px0}}} = 1 \tag{1b}$$

where

P -- axial force;

P_{P} -- axial plastic capacity of the CFT section, $P_{\mathrm{P}} = A_{\mathrm{s}} f_{\mathrm{y}} + A_{\mathrm{c}} f_{\mathrm{ck}}$;

M_{x} -- bending moment;

M_{Px0} -- plastic bending moment of the CFT section in case of no axial force;

f_{y} -- yield strength of steel;

f_{ck} -- characteristic strength of concrete;

A_{s} -- area of steel tube;

A_{c} -- area of concrete;

$$\alpha_{\mathrm{c}} = \frac{A_{\mathrm{c}} f_{\mathrm{ck}}}{P_{\mathrm{P}}}$$

Both the theoretical results based on full plasticity assumption and the curves of Eq. 1 are shown in Figure 1b. Eq. 1 is safe and simple, so it was included in the most widely applied software SATWE as a new type of cross section immediately after the issuing of CECS159-2004.

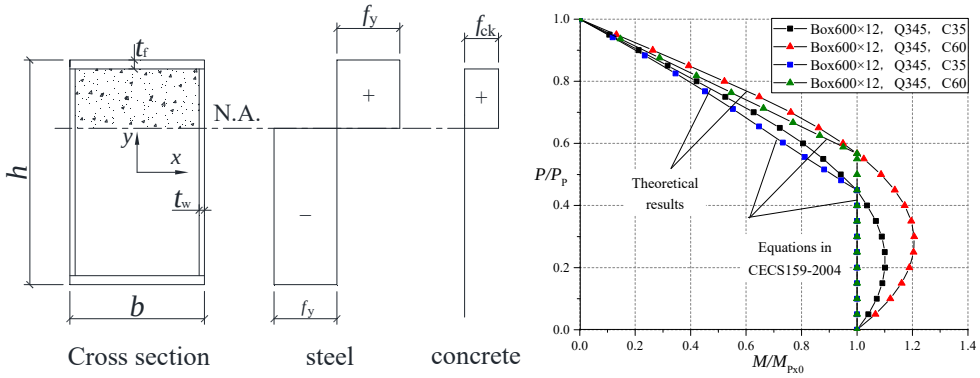

(a) analytical model (b) interaction curves

Figure 1. Comparison of Theoretical Results with CECS159-2004

Although a general method for computing the 3D strength surface is available, and the software XTRACT (Chadwell and Imbsen [9]) is free and has found application in the research work, there exists true need by the designers for simple design equations of L-shaped/T-shaped CFT sections. The present paper will address this need.

In recent years, several groups of researchers (Shen *et al*. [10]; Zuo *et al*. [11]; Zhang *et al*. [12]; Wang and Lv [13]) investigated the static and seismic behavior of L-shaped/T-shaped concrete-filled tube columns, including the local stability of the L-shaped/T-shaped tube, and the strengthening effect of penetrating binding bolts. Zuo *et al*. [11] computed the 3D strength of L-shaped CFT with equal legs and one thickness of the tube wall. Lei *et al*. [14] investigated T-shaped tubes with their total width identical to total depth. Both proposed complicated interaction equations for the combined action of axial force and biaxial bending and applicable only for the investigated shape of the cross section.

In this paper, the L-shaped CFT members are slightly different from the above studies in that the cross-section is composed of 3 rectangular and/or square tubes. A multi-celled tube column has the merit that the concrete in each cell is confined by its own tube so that the improvement in ductility may be estimated by currently available researches on square or rectangular CFTs. Also, the limit on the width-to-thickness ratio of the steel plate elements, specified for CFT members in CECS 159-2004, is directly applicable.

The maximum yield strength of concrete-filled L-shaped multi-celled tube column (abbreviated L-CFT hereafter) under axial force and uniaxial or biaxial bending is studied in this paper. L-shaped and T-shaped CFT cross sections comprise of 3(L) and 4(T) rectangular/square tubes, so it is assumed that the effect of confinement of steel tube toconcrete is assumed to produce only an increase in ductility of the concrete and no increase in strength (Hajjar and Gourley [7]), so uniform stress blocks are assumed both for the steel and the concrete as in the equations of CECS159-2004.

2 ULTIMATE STRENGTH UNDER UNIAXIAL ECCENTRIC LOAD

2.1 Elastic Properties of L-shaped Section

The sections of concrete-filled L-shaped multi-celled steel tube column investigated in this paper are shown in Figure 2, the section is composed of a flange box and a web box, the size of the flange box is $h_1 \times b_1$, the size of the web box is $h_2 \times b_2$, and they are actually composed of two different kinds of steel plates with thickness of t_1 and t_2. Each plate of the section is assigned a name as shown in Figure 2. The total width of L-shaped section is $b = h_1 + b_2$, the total height is $h = b_1 + h_2$, the steel tube is filled with concrete.

The origin of the coordinate system is first located at the left-bottom corner of the section shown in Figure 2. Both steel and concrete are elastic, the elastic modulus of them are E_s and E_c respectively. The elastic centroid of the section is located at Point $C(x_{sc}, y_{sc})$. The following assumptions are adopted: 1) The L-shaped CFT section obeys the Bernoulli's assumption; 2) In the full plastic hinge state, the steel reaches the compressive yield strength f_y, the compression concrete reaches its standard value of compressive yield strength f_{ck}, the tensile strength of concrete is ignored.

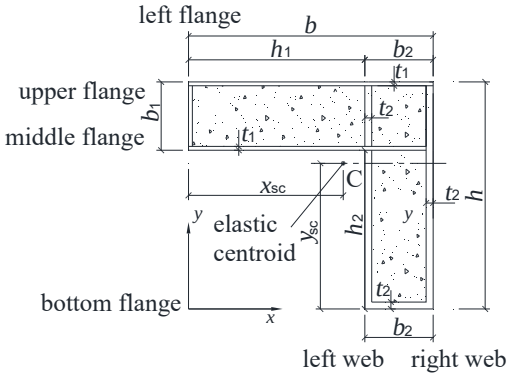

Figure 2. L-shaped Steel Tube Column Section

According to the parameters illustrated in Figure 2, the area of steel and concrete respectively in flange box and web box can be given by (c-concrete, s-steel, f-flange, w-web)

$$A_{\mathrm{cf}} = (b_1 - 2t_1)(b - t_1 - 2t_2) \tag{2a}$$

$$A_{\mathrm{sf}} = 2bt_1 + (b_1 - 2t_1)(t_1 + 2t_2) \tag{2b}$$

$$A_{\mathrm{cw}} = (h_2 - t_2)(b_2 - 2t_2) \tag{2c}$$

$$A_{\mathrm{sw}} = 2h_2t_2 + (b_2 - 2t_2)t_2 \tag{2d}$$

Denoting $\alpha_{\mathrm{E}} = E_{\mathrm{s}} / E_{\mathrm{c}}$, the transformed area of the section is

$$A_{\mathrm{tot}} = A_{\mathrm{sf}} + A_{\mathrm{sw}} + \frac{A_{\mathrm{cf}} + A_{\mathrm{cw}}}{\alpha_{\mathrm{E}}} \tag{3}$$

The coordinate of the elastic centroid $(x_{\mathrm{sc}}, y_{\mathrm{sc}})$ is

$$x_{\mathrm{sc}} = \frac{1}{A_{\mathrm{tot}}}\left\{\left[2ht_2 + (b_2 - 2t_2)(t_2 + 2t_1) + \frac{A_{\mathrm{cw}} + (b_1 - 2t_1)(b_2 - 2t_2)}{\alpha_{\mathrm{E}}}\right](b - \frac{1}{2}b_2)\right.$$
$$\left. + (h_1^2 - t_1^2)\left[t_1 + \frac{b_1 - 2t_1}{2\alpha_{\mathrm{E}}}\right] + \frac{1}{2}b_1{t_1}^2\right\} \tag{4a}$$

$$y_{\mathrm{sc}} = \frac{1}{A_{\mathrm{tot}}}\left\{\left(A_{\mathrm{sf}} + \frac{A_{\mathrm{cf}}}{\alpha_{\mathrm{E}}}\right)(h - \frac{1}{2}b_1) + (h_2 + t_2)\left[(h_2 - t_2)t_2 + \frac{A_{\mathrm{cw}}}{2\alpha_{\mathrm{E}}}\right] + \frac{1}{2}b_2{t_2}^2\right\} \tag{4b}$$

After the elastic centroid has been found, the origin of the coordinate system will be moved to the centroid. All properties and bending moments will be calculated about the centroid coordinate system.

The moment of inertia about the *x*- and *y*-axis are

$$I_{\mathrm{x}} = I_{\mathrm{x,bot}} - A_{\mathrm{tot}} y_{\mathrm{sc}}^2 \tag{5a}$$

$$\begin{aligned} I_{\mathrm{x,bot}} = {} & \left(\frac{A_{\mathrm{cf}}}{\alpha_{\mathrm{E}}} + A_{\mathrm{sf}} \right) \left(h - \frac{1}{2} b_1 \right)^2 + \frac{1}{12} b_1 (t_1^3 + 2t_2^3) + (b - t_1 - 2t_2) \left[t_1 \left(b_1 - t_1 \right)^2 + \frac{(b_1 - 2t_1)^3}{12\alpha_{\mathrm{E}}} \right] \\ & + \frac{1}{3} \left(2t_2 + \frac{b_2 - 2t_2}{\alpha_{\mathrm{E}}} \right) h_2^3 + \frac{1}{3} \left(1 - \frac{1}{\alpha_{\mathrm{E}}} \right) (b_2 - 2t_2) t_2^3 \end{aligned} \tag{5b}$$

$$I_{\mathrm{y}} = I_{\mathrm{y,bot}} - A_{\mathrm{tot}} x_{\mathrm{sc}}^2 \tag{5c}$$

$$\begin{aligned} I_{\mathrm{y,bot}} = {} & \left[\frac{(b_2 - 2t_2)(h - 2t_1 - t_2)}{\alpha_{\mathrm{E}}} + 2ht_2 + (2t_1 + t_2)(b_2 - 2t_2) \right] \left(b - \frac{1}{2} b_2 \right)^2 + \frac{1}{3} \left(1 - \frac{1}{\alpha_{\mathrm{E}}} \right) (b_1 - 2t_1) t_1^3 \\ & + \frac{1}{12} b_2 (2t_1^3 + t_2^3) + (h - 2t_1 - t_2) \left[t_2 \left(b_2 - t_2 \right)^2 + \frac{(b_2 - 2t_2)^3}{12\alpha_{\mathrm{E}}} \right] + \frac{1}{3} \left(2t_1 + \frac{b_1 - 2t_1}{\alpha_{\mathrm{E}}} \right) h_1^3 \end{aligned} \tag{5d}$$

$$I_{\mathrm{xy}} = I_{\mathrm{xy,bot}} - A_{\mathrm{tot}} x_{\mathrm{sc}} y_{\mathrm{sc}} \tag{5e}$$

$$\begin{aligned} I_{\mathrm{xy,bot}} = {} & \frac{1}{2} b^2 t_1 (h + h_2) + (b_1 - 2t_1)(h - \frac{1}{2} b_1)(\frac{1}{2} t_1^2 + h_1 t_2 + b t_2) + \frac{1}{2} t_2 h_2^2 (b + h_1) \\ & + \frac{1}{2} t_2^2 (b_2 - 2t_2)(b - \frac{1}{2} b_2) + \frac{1}{\alpha_{\mathrm{E}}} \left\{ (h - \frac{1}{2} b_1)(b_1 - 2t_1) \left[\frac{1}{2} (h_1^2 - t_1^2) + (b_2 - 2t_2)(b - \frac{1}{2} b_2) \right] \right. \\ & \left. + \frac{1}{2} (h_2 - t_2)(b_2 - 2t_2)(b - \frac{1}{2} b_2)(h_2 + t_2) \right\} \end{aligned} \tag{5f}$$

where $I_{\mathrm{x,bot}}$ is the moment of inertia around y=0, $I_{\mathrm{y,bot}}$ is the moment of inertia around x=0, $I_{\mathrm{xy,bot}}$ is the moment of inertia around the origin of the coordinate system.

When both steel and concrete of the section yield, the center of the axial compressive strength is located at $(x_{\mathrm{cc}}, y_{\mathrm{cc}})$ (measured from the left-bottom corner):

$$\begin{aligned} x_{\mathrm{cc}} = {} & \frac{1}{P_{\mathrm{p}}} \left\{ \left[2ht_2 f_{\mathrm{y}} + (b_2 - 2t_2)(2t_1 + t_2) f_{\mathrm{y}} + (b_2 - 2t_2)(h - 2t_1 - t_2) f_{\mathrm{ck}} \right] (b - \frac{1}{2} b_2) \right. \\ & \left. + t_1 h_1^2 f_{\mathrm{y}} + \frac{1}{2} (b_1 - 2t_1)(h_1^2 - t_1^2) f_{\mathrm{ck}} + \frac{1}{2} (b_1 - 2t_1) t_1^2 f_{\mathrm{y}} \right\} \end{aligned} \tag{6a}$$

$$y_{\mathrm{cc}} = \frac{1}{P_{\mathrm{p}}} \left\{ \left(A_{\mathrm{sf}} f_{\mathrm{y}} + A_{\mathrm{cf}} f_{\mathrm{ck}} \right) \left(h - \frac{b_1}{2} \right) + t_2 h_2^2 f_{\mathrm{y}} + \frac{1}{2} (b_2 - 2t_2)(h_2^2 - t_2^2) f_{\mathrm{ck}} + \frac{1}{2} (b_2 - 2t_2) t_2^2 f_{\mathrm{y}} \right\} \tag{6b}$$

The center of the axial tensile strength is located at (x_{tc}, y_{tc}) (measured from the left-bottom corner):

$$x_{tc} = \frac{1}{A_{sf} + A_{sw}} \left\{ \left[2ht_2 + (b_2 - 2t_2)(2t_1 + t_2) \right] (b - \frac{1}{2} b_2) + t_1 h_1^2 + \frac{1}{2} (b_1 - 2t_1) t_1^2 \right\} \tag{7a}$$

$$y_{tc} = \frac{1}{A_{sf} + A_{sw}} \left[A_{sf} \left(h - \frac{1}{2} b_1 \right) + t_2 h_2^2 + \frac{1}{2} (b_2 - 2t_2) t_2^2 \right] \tag{7b}$$

Introduce the following notations for axial forces and bending moments

$$P_s = (A_{sf} + A_{sw}) f_y \tag{8a}$$

$$P_c = (A_{cf} + A_{cw}) f_{ck} \tag{8b}$$

$$P_P = P_s + P_c \tag{8c}$$

$$\alpha_{ck} = P_c / P_p \tag{9}$$

$$M_{x,rc} = P_P (y_{cc} - y_{sc}) \tag{10a}$$

$$M_{x,rt} = P_s (y_{sc} - y_{tc}) \tag{10b}$$

$$M_{y,rc} = P_P (x_{cc} - x_{sc}) \tag{10c}$$

$$M_{y,rt} = P_s (x_{sc} - x_{tc}) \tag{10d}$$

where

P_s -- axial plastic capacity of the steel part of the L-CFT section;
P_c -- compressive capacity of the concrete part of the L-CFT section;
$M_{x,rc}$ -- the bending moment around the centroid axis *x* when the full L-CFT section yields in compression;
$M_{x,rt}$ -- the bending moment around the centroid axis *x* when the full L-CFT section yields in tension;
$M_{y,rc}$ -- the bending moment around the centroid axis *y* when the full L-CFT section yields in compression;
$M_{y,rt}$ -- the bending moment around the centroid axis *y* when the full L-CFT section yields in tension;
f_y -- yield strength of steel, $f_y = 235 \text{N/mm}^2$ and $f_y = 345 \text{N/mm}^2$ respectively in this paper;
f_{ck} -- standard value of compressive yield strength of concrete, C30-C60 (cubic strength) are adopted in this paper.

2.2 $P-M_x-M_{y,x}$ Curve of L-CFT Sections for the Plastic Neutral Axis Parallelled to x-axis

Uniaxial bending means that the plastic neutral axis is parallel to the centroid axis. Uniaxial bending around the *x* axis of the section will be studied first.

2.2.1 Characteristics of $P-M_x$ interaction curves

When a plastic hinge forms under the action of axial force and bending moment, the plastic neutral axis may be located in the upper flange, in the flange concrete, in the middle flange, in the web concrete or in the bottom flange. The axial force and the bending moment of the L-CFT section for these 5 cases can be written down respectively, they are not presented in this paper for brevity.

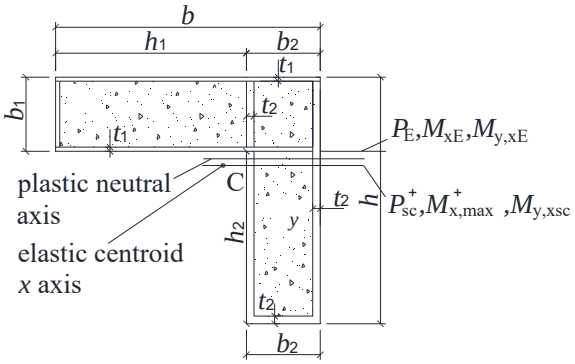

Figure 3. Interactive Relation of L-shaped Section when Plastic Neutral Axis is Parallel to the *x* axis

Let $M_{y,x}$ be the bending moment around the *y* axis when the plastic neutral axis is parallel to the *x* axis. Assume *P* (the axial force) is positive when it is compression, M_x is positive when it produces compressive stress in the upper flange, $M_{y,x}$ is positive when it produces compressive stress in the right web. As the plastic neutral axis is located in different locations, the axial forces and bending moments are given different notations, they are defined in Figure 3 and Table 1.

Table 1. Notations of Forces when Plastic Neutral Axis is Parallel to the *x* Axis

Forces	Position of plastic neutral axis
$P_t, M_{x,rt}, M_{y,rt}$	Full tension
$P_E, M_{xE}, M_{y,xE}$	Bottom surface of the middle flange
$P_P, M_{x,rc}, M_{y,rc}$	Full compression
$P_{sc}^+, M_{x,max}^+, M_{y,xsc}$	Elastic centroid *x* axis

After graphical presentations of the $P-M_x$ and $P-M_{y,x}$ curves for many different combinations of dimensional parameters and material strengths, a typical $P-M_x$ curve is identified and shown in Figure 4.

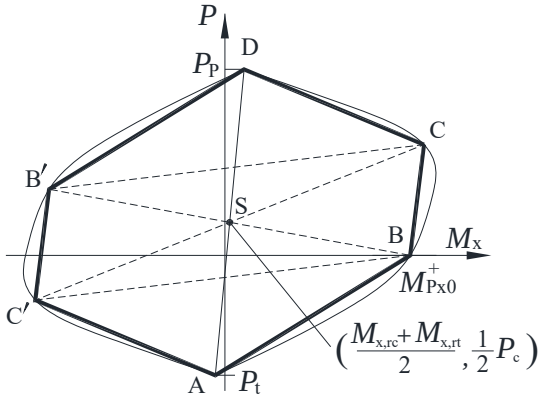

Figure 4. Geometric Symmetry Point of the $P-M_x$ Curves

There are 4 points on the curve:
Point A $(M_{x,rt}, -P_s)$: full tension

Point B $(M^+_{Px0}, 0)$: pure bending when the flange box in compression

Point C (M_C, P_C) : $P_C = \max(P_E, P^+_{sc}, P_c)$, M_C is the corresponding bending moment

Point D $(M_{x,rc}, P_P)$: full compression

We note that Point D is rotationally symmetric with Point A about Point S $\left(\frac{1}{2}(M_{x,rt}+M_{x,rc}), \frac{1}{2}P_c\right)$.

M^+_{Px0} is the plastic bending moment when the section is under pure bending around the *x* axis. P^+_{sc} is the axial force when the plastic neutral axis coincides with the elastic centroid axis *x*. It can been verified that at this location the plastic bending moment is maximum for any variation of the cross sections and any strength combinations of steel and concrete, and will be denoted by $M^+_{x,max}$.

The maximum negative moment is $(M^-_{x,max}, P^-_{sc})$ when the flange box is in tension and the plastic neutral axis coincides with the elastic centroid axis.

The centroid axis *x* divides the steel into two parts, A_{s+} and A_{s-}, and it divides the concrete into two parts, A_{c+} and A_{c-}. Referring to Figure 5, when the plastic neutral axis coincides with the elastic centroid axis, we have the follow relations.

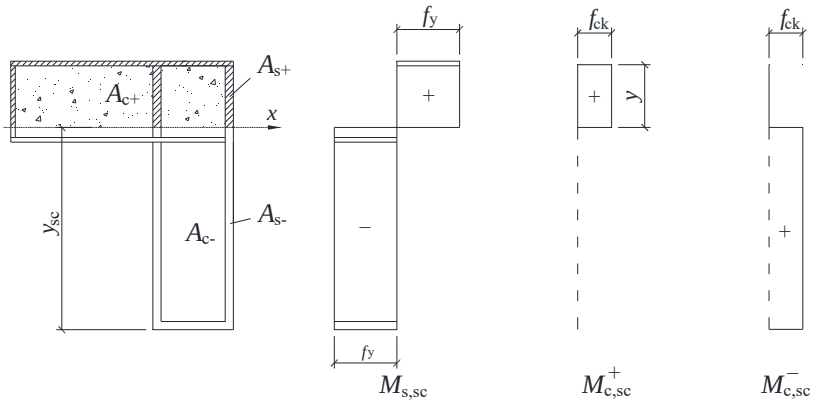

Figure 5. Plastic Moments when Plastic Neutral Axis Coincides with the Centroid Axis

The axial force and the bending moment when the flange box is in compression:

$$P_{sc}^{+}=(A_{s+}-A_{s-})f_y+A_{c+}f_{ck} \tag{11a}$$

$$M_{x,max}^{+}=f_y\left(\int_{A_{s+}}ydA-\int_{A_{s-}}ydA\right)+f_{ck}\int_{A_{c+}}ydA=M_{s,sc}+M_{c,sc}^{+} \tag{11b}$$

The axial force and the bending moment when the flange box is in tension:

$$P_{sc}^{-}=-(A_{s+}-A_{s-})f_y+A_{c-}f_{ck} \tag{11c}$$

$$M_{x,max}^{-}=-f_y\left(\int_{A_{s+}}ydA-\int_{A_{s-}}ydA\right)+f_{ck}\int_{A_{c-}}ydA=-M_{s,sc}+M_{c,sc}^{-} \tag{11d}$$

where $M_{s,sc}$ is the plastic moment of steel (Figure 5b);

$M_{c,sc}^{+}$ is the plastic moment of concrete above the centroid axis (Figure 5c);

$M_{c,sc}^{-}$ is the plastic moment of concrete below the centroid axis (Figure 5c);

These moments are provided by stresses in steel and concrete shown in Figure 5.

$$M_{s,sc}=f_y\left(\int_{A_{s+}}ydA-\int_{A_{s-}}ydA\right)=M_{s,sc}^{+}+M_{s,sc}^{-} \tag{12a}$$

$$M_{c,sc}^{+}=f_{ck}\int_{A_{c+}}ydA \tag{12b}$$

$$M_{s,sc}^{+}=f_y\int_{A_{s+}}ydA \tag{12c}$$

$$M_{s,sc}^{-}=-f_y\int_{A_{s-}}ydA \tag{12d}$$

$$P_{sc}^{+}=(A_{s+}-A_{s-})f_y+A_{c+}f_{ck} \tag{12e}$$

Because $P_{sc}^{+}+P_{sc}^{-}=A_c f_{ck}=P_c$, so one has

$$P_{sc}^{+}-0.5P_c=0.5P_c-P_{sc}^{-} \tag{13a}$$

Summation of two maximum bending moments

$$M_{x,max}^{+}+M_{x,max}^{-}=f_{ck}\int_{A_{c+}}ydA+f_{ck}\int_{A_{c-}}ydA=M_{c,sc}^{+}+M_{c,sc}^{-}=S_{x,c}f_{ck} \tag{13b}$$

where $S_{x,c}=\int_{A_c}ydA$.

When the cross section is in full tension and in compression, the bending moments are

$$M_{x,rt}=-f_y\int_{A_{s+}}ydA-f_y\int_{A_{s-}}ydA=-M_{s,sc}^{+}+M_{s,sc}^{-}=-S_{x,s}f_y \tag{14a}$$

$$M_{x,rc}=S_{x,s}f_y+S_{x,c}f_{ck}=-M_{x,rt}+M_{c,sc}^{+}+M_{c,sc}^{-} \tag{14b}$$

where $S_{x,s}=\int_{A_s}ydA$

Thus

$$M_{x,rt}+M_{x,rc}=M_{c,sc}^{+}+M_{c,sc}^{-}=M_{x,max}^{+}+M_{x,max}^{-} \tag{14c}$$

So Point $(M_{x,max}^{-},P_{sc}^{-})$ is rotationally symmetric with the maximum positive moment $(M_{x,max}^{+},P_{sc}^{+})$ about Point S$\left(\frac{1}{2}(M_{x,rt}+M_{x,rc}),\frac{1}{2}P_c\right)$.

For any location of the plastic neutral axis (Figure 6), $A'_{s+},A'_{s-},A'_{c+},A'_{c-}$ are the steel and concrete areas above and below the neutral axis. The axial force and bending moment when the upper flange is in compression are

$$P^{+}=(A'_{s+}-A'_{s-})f_y+A'_{c+}f_{ck} \tag{15a}$$

$$M_x^{+}=f_y\left(\int_{A'_{s+}}ydA-\int_{A'_{s-}}ydA\right)+f_{ck}\int_{A'_{c+}}ydA \tag{15b}$$

the axial force and the bending moment when the web concrete is in compression are

$$P^{-}=-(A'_{s+}-A'_{s-})f_y+A'_{c-}f_{ck} \tag{15c}$$

$$M_x^{-}=-f_y\left(\int_{A'_{s+}}ydA-\int_{A'_{s-}}ydA\right)+f_{ck}\int_{A'_{c-}}ydA \tag{15d}$$

and

$$P^+ + P^- = P_c$$

$$M_x^+ + M_x^- = f_{ck}\int_{A_{c+}'} ydA + f_{ck}\int_{A_{c-}'} ydA = S_{x,c}\, f_{ck}$$

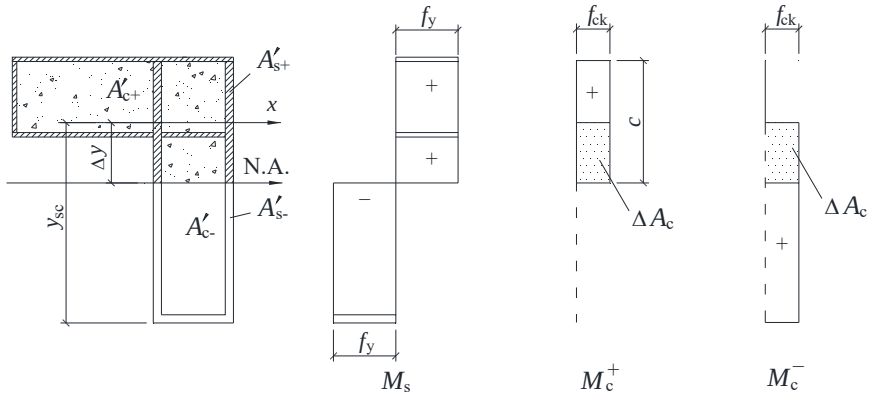

Figure 6. Plastic Moments for Different Location of the Plastic Neutral Axis

so we have

$$P^+ - 0.5P_c = 0.5P_c - P^- \tag{16a}$$

$$M_c^+ + M_c^- = M_{c,sc}^+ + M_{c,sc}^- = M_{x,rt} + M_{x,rc} = M_{x,max}^+ + M_{x,max}^- \tag{16b}$$

So we have verified that the left of the $P - M_x$ curves in Figure 4 is rotationally symmetric with the right of the $P - M_x$ curves about Point $\mathrm{S}\left(\frac{1}{2}(M_{x,rt} + M_{x,rc}), \frac{1}{2}P_c\right)$.

The pure bending plastic moment is M_{Px0}^- when the flange concrete is in tension. The rotationally symmetric Point of $(M_{Px0}^-, 0)$ on the right of Figure 4 is (M_c, P_c), and

$$M_c = -M_{Px0}^- + (M_{x,rt} + M_{x,rc}) \tag{17}$$

Extensive examples show that $M_{c,sc}^+ + M_{c,sc}^-$ are small quantities, and

$$\frac{M_{x,max}^+}{M_{x,max}^-} = 1 \pm 0.02 \tag{18}$$

2.2.2 Determination of Point C and Point E

Except Point $\mathrm{A}(M_{x,rt}, -P_s)$, Point $\mathrm{B}(M_{Px0}^+, 0)$ and Point $\mathrm{D}(M_{x,rc}, P_p)$, the following 3 points will be

used to define Point C on the $P-M_x$ curves:
(M_{xE}, P_E), $(M^+_{x,max}, P^+_{sc})$ and (M_c, P_c)

Many $P-M_x$ interaction curves are obtained, several typical curves are shown in Figure 7, they are plotted with m_x as the abscissa against *p* as the ordinate, where

$$m_x = \frac{M_x}{M^+_{Px0}} \tag{19a}$$

$$p = \frac{P}{P_P} \tag{19b}$$

Six cases are identified and are listed in Table 2 according to the relative positions of the elastic centroid axis *x* and the plastic neutral axis under pure bending around the *x* axis. The relative values of axial forces for these 6 cases are also given in Table 2.

Table 2. Classification of Section Type

Case No	Position of plastic neutral axis under pure bending	Position of elastic centroid axis *x*	Maximum of P_E, P_c, P^+_{sc} (Point C)	Figure
Case1a	Flange concrete	Flange concrete	P_E	Figure 7a
Case1b		Middle flange	P_E	Figure 7b
Case1c		Web concrete	P^+_{sc}	Figure 7c
Case2a	Middle flange	Middle flange	P_E	Figure 7d
Case2b		Web concrete	P_c	Figure 7e
Case3	Web concrete	Web concrete	P_c	Figure 7f

In Figure 7, the axial force at Point C is

$$P_C = \max(P_E, P^+_{sc}, P_c) \tag{20a}$$

M_{xC} are the bending moments corresponding to P_C (i.e. if $P_C = \max(P_E, P^+_{sc}, P_c) = P_E$, then $M_{xC} = M_{xE}$; if $P_C = \max(P_E, P^+_{sc}, P_c) = P_c$, then $M_{xC} = M_c = -M^-_{Px0}$). The axial forces at Point C of these 6 cases are listed in Table 2.

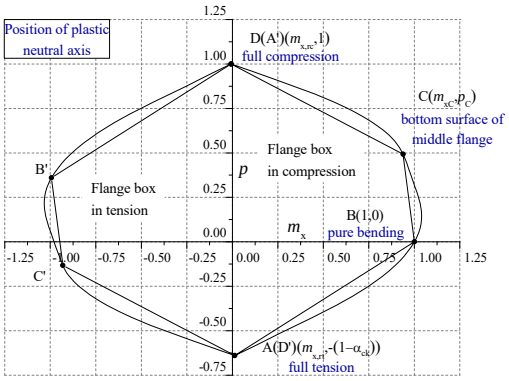

FB160x160x6,WB160x160x6,C40,Q345

(a1) $p-m_x$ curve of Case1a

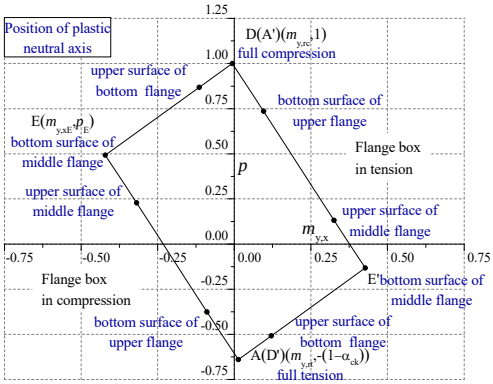

FB160x160x6,WB160x160x6,C40,Q345

(a2) $p-m_{y,x}$ curve of Case1a

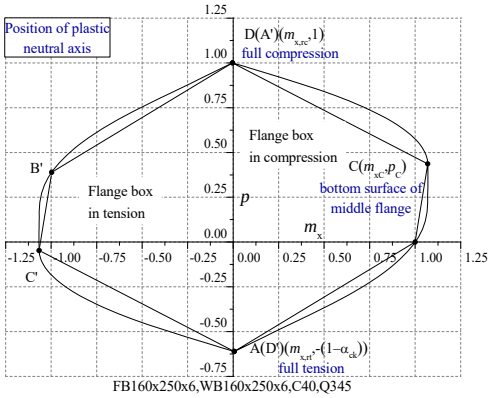

FB160x250x6,WB160x250x6,C40,Q345

(b1) $p-m_x$ curve of Case1b

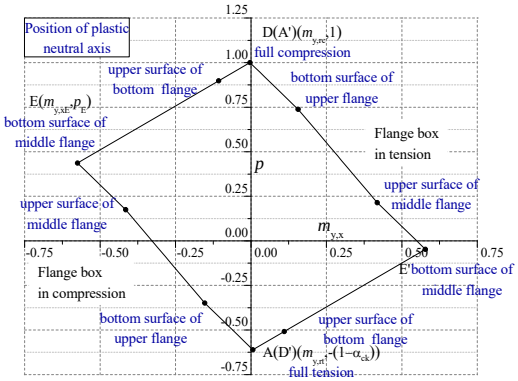

FB160x250x6,WB160x250x6,C40,Q345

(b2) $p-m_{y,x}$ curve of Case1b

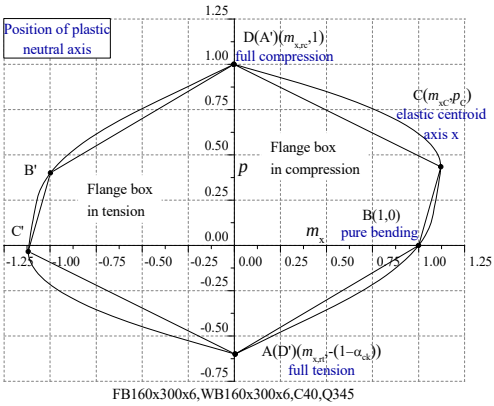

FB160x300x6,WB160x300x6,C40,Q345

(c1) $p-m_x$ curve of Case1c

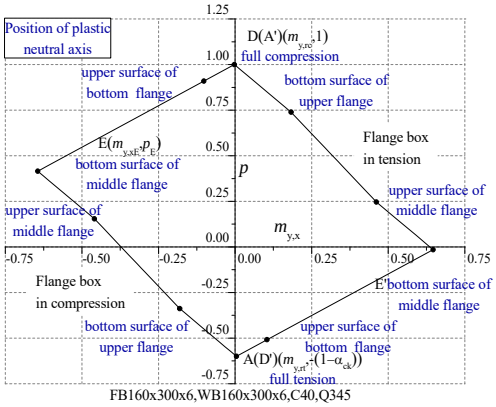

FB160x300x6,WB160x300x6,C40,Q345

(c2) $p-m_{y,x}$ curve of Case1c

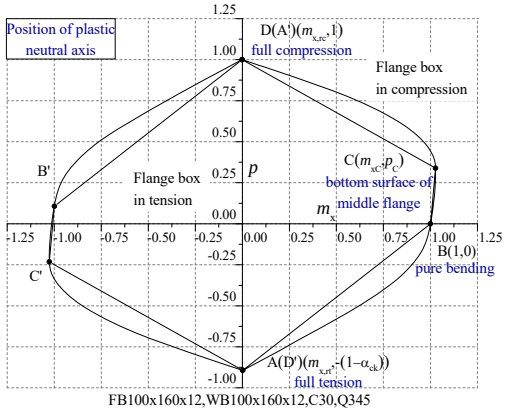

(d1) $p-m_x$ curve of Case2a

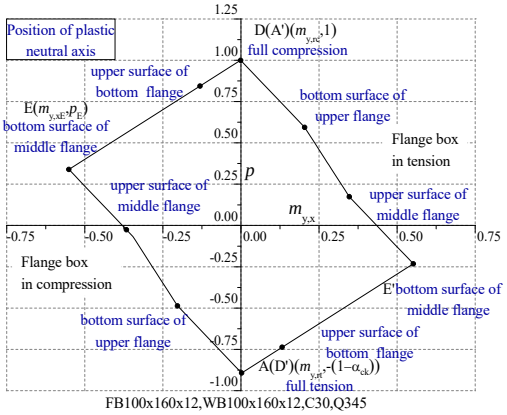

(d2) $p-m_{y,x}$ curve of Case2a

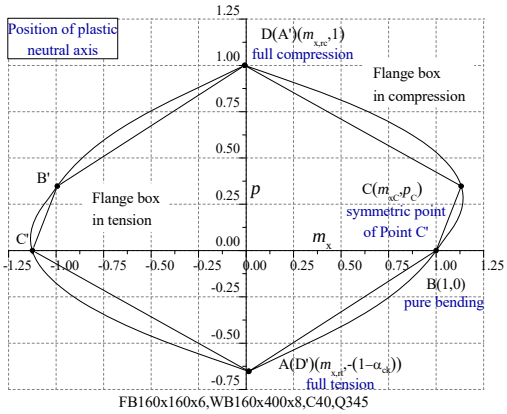

(e1) $p-m_x$ curve of Case2b

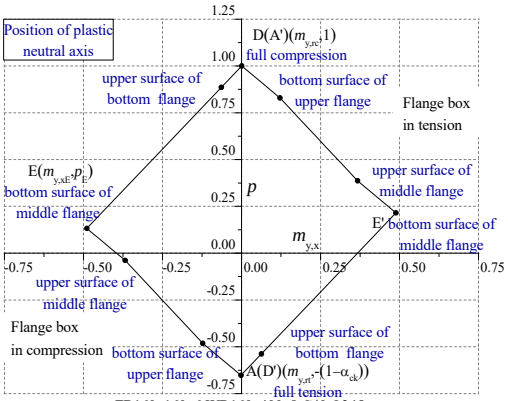

(e2) $p-m_{y,x}$ curve of Case2b

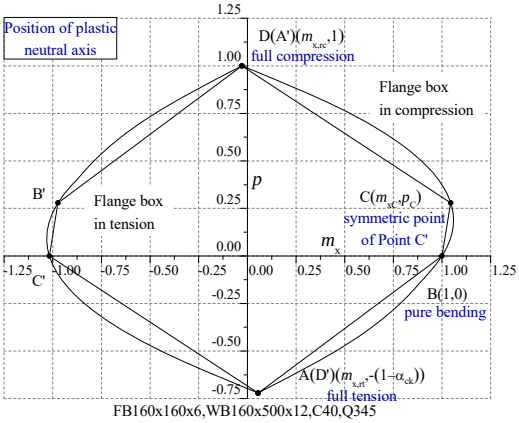

(f1) $p-m_x$ curve of Case3

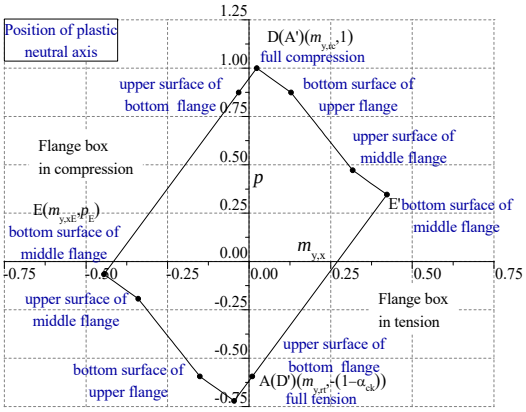

(f2) $p-m_{y,x}$ curve of Case3

Figure 7. Interaction Curves of L-shaped Section when Plastic Neutral Axis is Parallel to the *x*-axis (Notation: FB $h_1\times b_1\times t_1$, WB $h_2\times b_2\times t_2$, FB=flange box, WB=web box)

According to the characteristics mentioned above, for these six cases, we can use piecewise linear model ABCD to express the $p-m_x$ curve when the section is under uniaxial compression and bending around *x*-axis as

Line A-B: $$-\frac{1-m_{\mathrm{x,rt}}}{1-\alpha_{\mathrm{ck}}}p+m_{\mathrm{x}}=1 \tag{21a}$$

Line B-C: $$\frac{1-m_{\mathrm{xC}}}{p_{\mathrm{C}}}p+m_{\mathrm{x}}=1 \tag{21b}$$

Line C-D: $$p+\frac{1-p_{\mathrm{C}}}{m_{\mathrm{xC}}-m_{\mathrm{x,rc}}}(m_{\mathrm{x}}-m_{\mathrm{x,rc}})=1 \tag{21c}$$

where

$$m_{\mathrm{x,rt}}=\frac{M_{\mathrm{x,rt}}}{M^{+}_{\mathrm{Px0}}},\ m_{\mathrm{x,rc}}=\frac{M_{\mathrm{x,rc}}}{M^{+}_{\mathrm{Px0}}},\ p_{\mathrm{C}}=\frac{P_{\mathrm{C}}}{P_{\mathrm{P}}},\ m_{\mathrm{xC}}=\frac{M_{\mathrm{xC}}}{M^{+}_{\mathrm{Px0}}} \tag{22}$$

The interaction curves of the axial force *P* and the accompanying bending moment $M_{\mathrm{y,x}}$ are also shown in Figure 7, they are plotted with $m_{\mathrm{y,x}}$ as the abscissa against *p* as the ordinate, where

$$m_{\mathrm{y,x}}=\frac{M_{\mathrm{y,x}}}{M^{+}_{\mathrm{Py0}}} \tag{23}$$

where M^{+}_{Py0} is the plastic bending moment when the section is under pure bending around the *y*-axis and the web box is in compression, it is calculated by a similar method as M^{+}_{Px0}.

There are three key points for each curve shown in Figure 7(a2, b2, c2, d2, e2, f2), the bending moment $M_{\mathrm{y,x}}$ and the axial force *P* at each point can be represented by

$$\mathrm{A}(M_{\mathrm{y,rt}},-P_{\mathrm{s}}),\ \mathrm{E}(M_{\mathrm{y,xE}},P_{\mathrm{E}}),\ \mathrm{D}(M_{\mathrm{y,rc}},P_{\mathrm{P}})$$

where Point E is related to the plastic neutral axis at the bottom surface of the middle flange (see in Table 1).

After that, we can use piecewise linear model AED to express the $p-m_{\mathrm{y,x}}$ curves in Figure 7 as

Line A-E: $$\alpha_{\mathrm{ck}}-p-\frac{\alpha_{\mathrm{ck}}-1-p_{\mathrm{E}}}{m_{\mathrm{y,xE}}-m_{\mathrm{y,rt}}}\left(m_{\mathrm{y,x}}-m_{\mathrm{y,rt}}\right)=1 \tag{24a}$$

Line E-D: $$p+\frac{1-p_{\mathrm{E}}}{m_{\mathrm{y,xE}}-m_{\mathrm{y,rc}}}\left(m_{\mathrm{y,x}}-m_{\mathrm{y,rc}}\right)=1 \tag{24b}$$

In Figure 7(a2, b2, c2, d2, e2, f2), the bending moment $M_{\mathrm{y,x}}$ and the axial force *P* at Points A′-D′ are also rotationally symmetrical with Points A-D about the point $\left(\frac{1}{2}(M_{\mathrm{y,rt}}+M_{\mathrm{y,rc}}),\frac{1}{2}P_{\mathrm{c}}\right)$.

After the right of the $P-M_{\mathrm{x}}$ and $P-M_{\mathrm{y,x}}$ curves have been formulated, the left of these curves can be found using the rotational symmetry. Similarly, the $P-M_{\mathrm{y}}-M_{\mathrm{x,y}}$ curve can be found when the plastic neutral axis is parallel to the *y*-axis.

2.2.3 Simplified equations for practical application

Designers truly need simple design equations for L-shaped and T-shaped CFTs, so we simplify Eq. 21 and Eq. 24 for practical application.

Based on the results of a large number of examples, when the section is in full tension, we take the coordinate of Point A as $(0,-P_{\mathrm{s}})$ approximately. When the section is in full compression, we take the coordinate of Point D as $(0,P_{\mathrm{p}})$.

So Eq. 21 can be simplified as

Line A-B: $$-\frac{P}{P_{\mathrm{s}}}+\frac{M_{\mathrm{x}}}{M_{\mathrm{Px0}}^{+}}=1 \tag{25a}$$

Line B-C: $$\left(1-\frac{M_{\mathrm{xC}}}{M_{\mathrm{Px0}}^{+}}\right)\frac{P}{P_{\mathrm{C}}}+\frac{M_{\mathrm{x}}}{M_{\mathrm{Px0}}^{+}}=1 \tag{25b}$$

Line C-D: $$\frac{P}{P_{\mathrm{P}}}+\left(1-\frac{P_{\mathrm{C}}}{P_{\mathrm{P}}}\right)\frac{M_{\mathrm{x}}}{M_{\mathrm{xC}}}=1 \tag{25c}$$

Eq. 24 can be simplified as

Line A-E: $$-\frac{P}{P_{\mathrm{s}}}+\left(1+\frac{P_{\mathrm{E}}}{P_{\mathrm{s}}}\right)\frac{M_{\mathrm{y,x}}}{M_{\mathrm{y,xE}}}=1 \tag{26a}$$

Line E-D: $$\frac{P}{P_{\mathrm{P}}}+\left(1-\frac{P_{\mathrm{E}}}{P_{\mathrm{P}}}\right)\frac{M_{\mathrm{y,x}}}{M_{\mathrm{y,xE}}}=1 \tag{26b}$$

Obviously, Eq. 25 and Eq. 26 are simple enough and can be used by designers conveniently.

3. $P-M_{\mathrm{x}}-M_{\mathrm{y}}$ RELATIONS OF L-CFT SECTIONS

An ultimate yield surface of the L-CFT section under biaxial bending and axial force is shown in Figure 8, the curves are plotted with m_{x} as the abscissa and m_{y} as the ordinate for a given axial force ratio *p*.

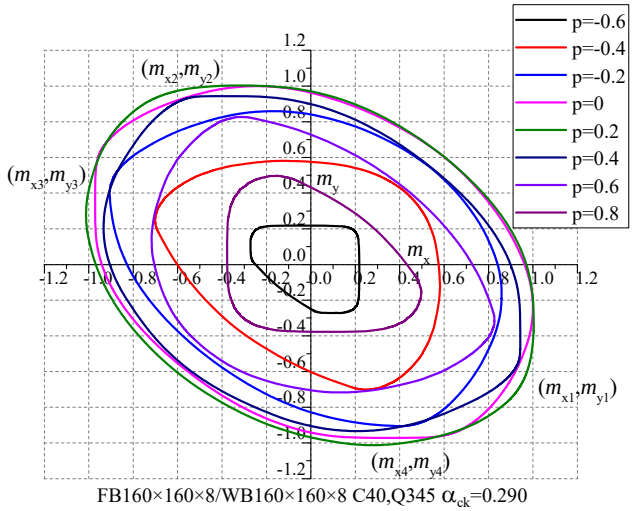

Figure 8. $m_x - m_y$ Curves of L-shaped Section under Biaxial Bending and Axial Force

There are 4 key points on each $m_x - m_y$ curve for a prescribed value of p, the coordinates of these 4 key points are given as (m_{xi}, m_{yi}), $i = 1,2,3,4$:

Point (m_{x1}, m_{y1}) is the right-most point of each curve,
Point (m_{x2}, m_{y2}) is the highest point of each curve,
Point (m_{x3}, m_{y3}) is the left-most point of each curve,
Point (m_{x4}, m_{y4}) is the negative highest point of each curve.

It has been found that they are points when the plastic neutral axis is parallel to the x axis or the y axis, so they can be calculated by equations presented in Section 2.

Figure 9(a) shows a plastic neutral axis passing through a rectangular section, the upper part is in compression. If it is a concrete section, the axial force and bending moment are

$$P = 2b(d-e) f_{ck} \tag{27a}$$

$$M_x = bf_{ck}\left[d^2 - (e + b\tan\theta)^2\right] + 2b^2 f_{ck}\left(e\tan\theta - \frac{2}{3}b\tan^2\theta\right) \tag{27b}$$

$$M_y = \frac{2}{3}b^3 f_{ck}\tan\theta \tag{27c}$$

when the parameter e is unchanged, and the neutral axis crosses two vertical boundaries, then the axial force is constant.

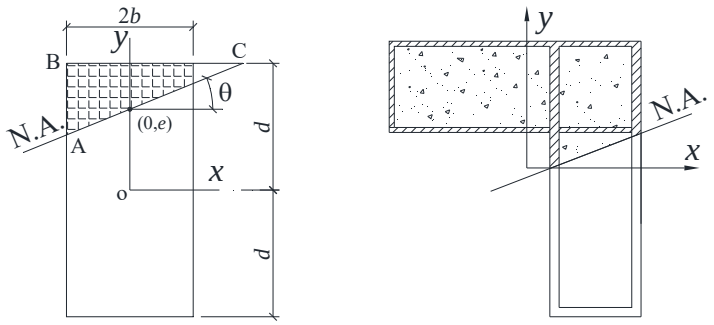

Figure 9. The Influence of Plastic Neutral Axis on the Axial Force and Bending Moment

Differentiate M_x with respect to θ, and let the derivative be zero:

$$\frac{dM_x}{d\theta}=\left[-2b^2\left(e+b\tan\theta\right)f_{ck}+2b^2f_{ck}\left(e-\frac{4}{3}b\tan\theta\right)\right]\frac{1}{\cos^2\theta}=0$$

from which, we obtain $\theta=0$.

The second derivative is

$$\frac{d^2M_x}{d\theta^2}=\left(-2b^3f_{ck}-\frac{8}{3}b^3f_{ck}\right)\frac{1}{\cos^2\theta}+\left[-2b^2\left(e+b\tan\theta\right)f_{ck}+2b^2\left(e-\frac{4}{3}b\tan\theta\right)f_{ck}\right]\frac{2\sin\theta}{\cos^3\theta}$$

and its value at $\theta=0$ is

$$\left.\frac{d^2M_x}{d\theta^2}\right|_{\theta=0}=-2b^3f_{ck}-\frac{8}{3}b^3f_{ck}<0$$

That is, when the plastic neutral axis is parallel to the *x* axis, M_x is a maximum. If the rectangle is in steel, this conclusion is also valid, and M_x is either a maximum or a minimum (negative maximum).

Figure 9(b) shows the L-shaped CFT section with a sloped neutral axis and the coordinate system. From the above derivation it can be deduced that for the L-shaped CFT section, when the plastic neutral axis is parallel to the *x* or *y* axis, the bending moment is either a maximum or a minimum under a prescribed axial force, because the L-CFT section can be seen a combination of several rectangular steel and concrete subsections.

Points (m_{xi},m_{yi}) divide the m_x-m_y curves into four segments, they can be fitted by

On the upper right side $m_{x2}\le m_x\le m_{x1},m_{y1}\le m_y\le m_{y2}$:

$$\left(\frac{m_x-m_{x2}}{m_{x1}-m_{x2}}\right)^{2-p}+\left(\frac{m_y-m_{y1}}{m_{y2}-m_{y1}}\right)^{2-p}=1 \tag{28a}$$

On the upper left side $m_{x3} \le m_x \le m_{x2}, m_{y3} \le m_y \le m_{y2}$:

$$\left(\frac{m_{x2}-m_x}{m_{x2}-m_{x3}}\right)^{1.6+\frac{1}{2}p}+\left(\frac{m_y-m_{y3}}{m_{y2}-m_{y3}}\right)^{1.6+\frac{1}{2}p}=1 \tag{28b}$$

On the lower right side $m_{x4} \le m_x \le m_{x1}, m_{y4} \le m_y \le m_{y4}$:

$$\left(\frac{m_x-m_{x4}}{m_{x1}-m_{x4}}\right)^{2-p}+\left(\frac{m_{y1}-m_y}{m_{y1}-m_{y4}}\right)^{2-p}=1 \tag{28c}$$

On the lower left side $m_{x3} \le m_x \le m_{x4}, m_{y4} \le m_y \le m_{y3}$:

$$\left(\frac{m_{x4}-m_x}{m_{x4}-m_{x3}}\right)^{1.6+\frac{2}{3}p}+\left(\frac{m_{y3}-m_y}{m_{y3}-m_{y4}}\right)^{1.6+\frac{2}{3}p}=1 \tag{28d}$$

Table 3. Parameters of Examples

Num	Flange box section/mm	Web box section/mm	$f_{ck}\left(\mathrm{N/mm^2}\right)$	$f_y\left(\mathrm{N/mm^2}\right)$	α_{ck}
1	160×160×8	160×160×8	26.8	345	0.290
2	200×200×6	200×200×6	26.8	345	0.418
3	100×200×6	100×350×6	26.8	345	0.301
4	200×400×8	200×700×12	20.1	235	0.359
5	200×400×8	250×450×10	38.5	235	0.568
6	250×350×6	200×400×8	20.1	235	0.462
7	100×250×6	100×250×6	38.5	235	0.471
8	200×400×8	200×400×10	38.5	235	0.539

Table 3 list 8 L-CFT sections with different values of f_{ck} and f_y, they are adopted to check the accuracy of Eq. 28. In Figure 10, solid lines show theoretical results based on full plasticity assumption, they are compared with Eq. 28 which are represented by dot lines, good agreements are achieved.

Eq. 28 can be used to calculate the ultimate yield surfaces of L-CFT of different parameters, it should be noted that the width-to-thickness of the section need to be limited to prevent the local plate buckling. Both flange and web box are required to satisfy $\left(\frac{b_1}{t_1},\frac{h_1}{t_1},\frac{b_2}{t_2},\frac{h_2}{t_2}\right) \le 60\sqrt{235/f_y}$.

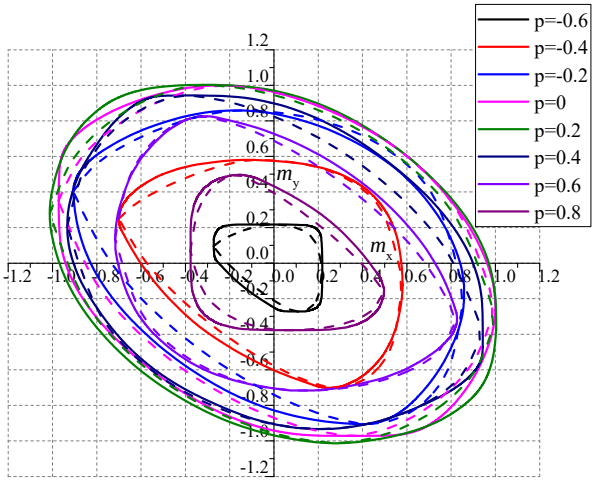

FB160×160×8/WB160×160×8 C40,Q345 α_{ck}=0.290

(a)

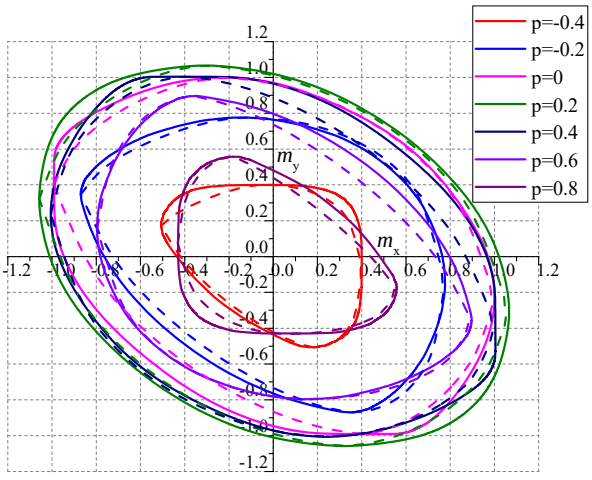

FB200×200×6/WB200×200×6 C40,Q345 α_{ck}=0.418

(b)

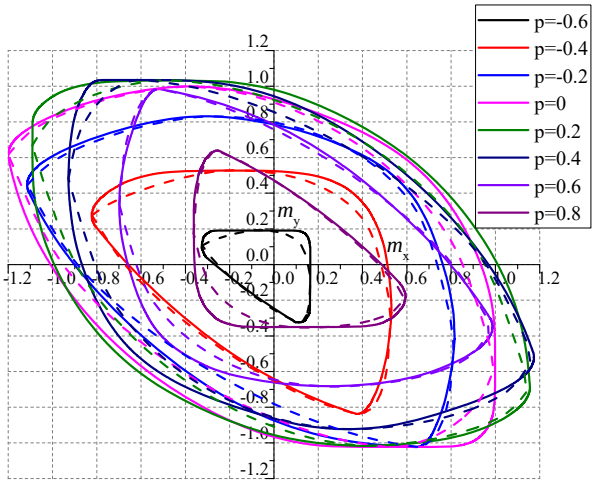

FB100×200×6/WB100×350×6 C40,Q345 α_{ck}=0.301

(c)

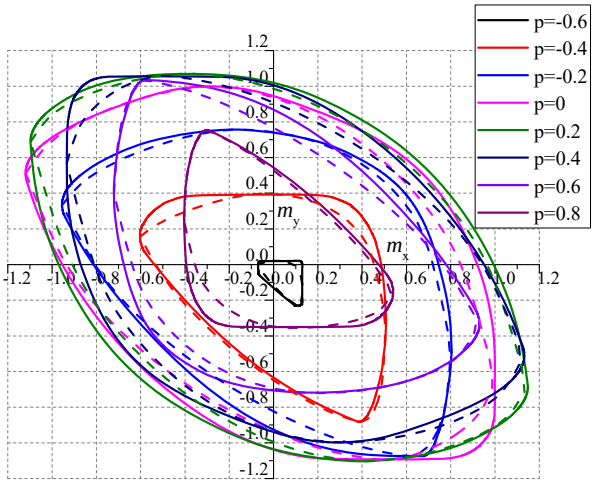

FB200×400×8/WB200×700×12 C30,Q235 α_{ck}=0.359

(d)

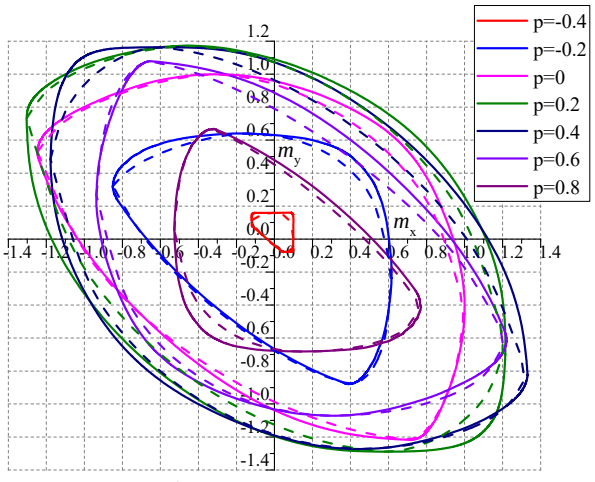

FB200×400×8/WB200×450×10 C60,Q235 α_{ck}=0.568

(e)

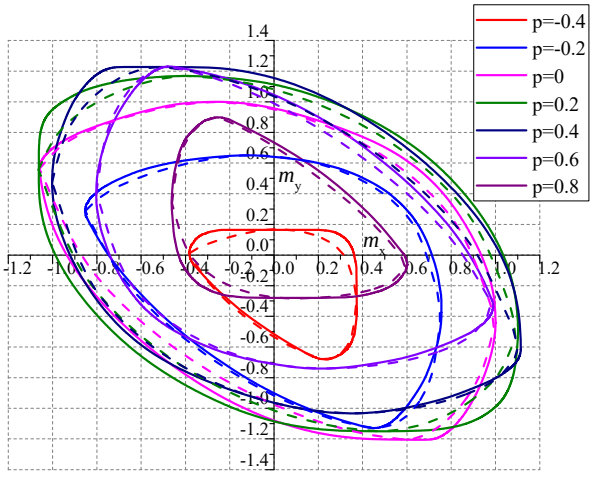

FB250×350×6/WB200×400×8 C30,Q235 α_{ck}=0.462

(f)

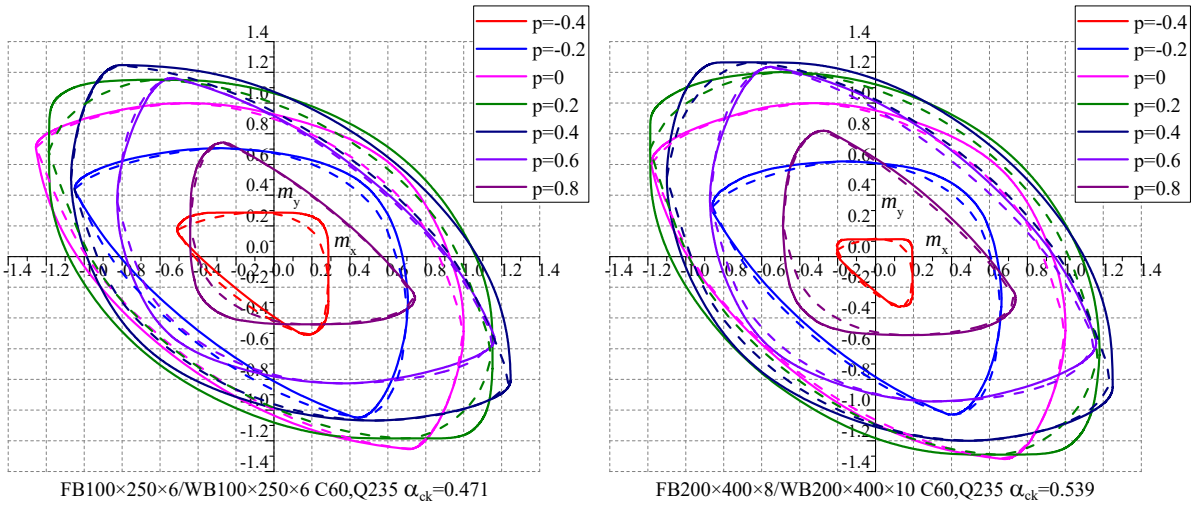

Figure 10. Comparison of Theoretical Results with Eq. 28
(Solid line: Theoretical Results, Dotted Line: Eq. 28

4. CONCLUSION

The maximum yield strength of concrete filled L-shaped tube section under biaxial bending and axial force was studied. In the maximum strength state, the steel reaches its yielding strength while the concrete reaches its characteristic strength of compression with neglecting the part under tension.

First the plastic strengths under uniaxial compression and bending are investigated, the characteristics of the axial force-bending moment interaction curves are revealed, the rotational symmetry of the whole interaction curve is verified mathematically. Results show that when the L-CFT section is under uniaxial compression and bending around the *x* axis, there are 6 cases according to the positions of elastic centroid axis and plastic neutral axis under pure bending, $P-M_x$ and $P-M_{y,x}$ curves are approximated by multilinear expressions respectively using the values (P, M_x, $M_{y,x}$) of the key points in different positions of plastic neutral axis.

Under axial force and biaxial bending of L-CFT section, a series of m_x-m_y curves under different axial force ration p are presented. Examples show that the ultimate bending moment around *x* and *y* axis is maximum when the plastic neutral axis is parallel to *x* and *y* axis respectively, this characteristic is also verified mathematically. These maximum points are then used to help formulate the $p-m_x-m_y$ equations of the L-CFT section. According to the comparison of a large number of examples, the proposed formulas are accurate enough and on the safe side.

ACKNOWLEDGMENT

The authors are grateful to the financial support from the National Key Research and Development Program of China through the grant No. 2016YFC0701201.

REFERENCES

[1] JGJ149-2006, "Technical Specification for Concrete Structures with Specially Shaped Columns". The Ministry of Housing and Urban-Rural Development of China: Beijing, 2006.
[2] Hsu, C.T.T., "T-shaped Reinforced Concrete Members under Biaxial Bending and Axial Compression", Aci Structural Journal, 1989, Vol. 86, No. 4, pp. 460-468.
[3] Hsu, C.T.T., "Biaxially Loaded L-shaped Reinforced Concrete Columns", Journal of Structural Engineering, 1985, Vol. 111, No. 12, pp. 2576-2595.
[4] Sun, J.H., "Lateral Stiffness and Analysis of Frames Built of Special Shaped Columns", Zhejiang University: Hangzhou, 2003.
[5] Zhao, Y.H., "Study on Bearing Capacity for SRC Special Shaped Columns", Xi'an University of Architecture and Technology: Xi'an, 2007.
[6] Chen, W.F. and Atsuta, T., "Theory of Beam-columns", McGraw-Hill: New York, 1976.
[7] Hajjar, J.F. and Gourley, B.C., "Representation of Cconcrete-filled Steel Tube Cross-section Strength", Journal of Structural Engineering, 1996, Vol. 122, No. 11, pp. 1327-1336.
[8] CECS159-2004, "Technical Specification for Structures with Concrete Filled Rectangular Steel Tube Members". The Ministry of Housing and Urban-Rural Development of China: Beijing, 2004.
[9] Chadwell, C.B. and Imbsen, R.A., "XTRACT: A Tool for Axial Force-ultimate Curvature Interactions", Structures Congress, ASCE, 2004.
[10] Shen, Z.Y., Lei, M., Li, Y.Q. and Luo, J.H., "Experimental Study on Seismic Behavior of Concrete-filled L-shaped Steel Tube Columns", Advances in Structural Engineering, 2013, Vol. 16, No. 7, pp. 1235-1248.
[11] Zuo, Z.L., Cai, J., Yang, C. and Chen, Q.J., "Eccentric Load Behavior of L-shaped CFT Stub Columns with Binding Bars", Journal of Constructional Steel Research, 2012, Vol. 72, No. 5, pp. 105-118.
[12] Zhang, J.C., Shen, Z.Y., Lin, Z.Y., and Luo, J.H., "Experimental Research on Seismic Behavior of Concrete-filled L-section Steel Tubular Frames", Journal of Building Structures, 2010, Vol. 31, No. 8, pp. 1-7.
[13] Wang, D. and Lv, X.L., "Experimental Study on Seismic Behavior of Concrete-filled Steel T-section and L-section Columns", Journal of Building Structures, 2005, Vol. 26, No. 4, pp. 39-44.
[14] Lei, M., Shen, Z.Y., Li, Y.Q. and Luo, J.H., "Sectional Strength of Concrete-filled T-shaped Steel Tube Column Subjected to Axial Compression and Bending Moment", Journal of Tongji University, 2016, Vol. 44, No. 3, pp. 348-354.